Journal of Alloys and Compounds 972 (2024) 172891

Contents lists available at ScienceDirect

Journal of Alloys and Compounds

journal homepage: www.elsevier.com/locate/jalcom

Deposition and in-situ formation of nanostructured Mo_2C nanoparticles on graphene nanowalls support for efficient electrocatalytic hydrogen evolution

Stefanos Chaitoglou [a,b,*], Rogelio Ospina [a,b,c], Yang Ma [a,b], Roger Amade [a,b], Xavier Vendrell [d], Jhonatan Rodriguez-Pereira [e,f], Enric Bertran-Serra [a,b]

[a] Department of Applied Physics, University of Barcelona, C/Martí i Franquès, 1, 08028 Barcelona, Catalunya, Spain
[b] ENPHOCAMAT Group, Institute of Nanoscience and Nanotechnology (IN2UB), University of Barcelona, C/Martí i Franquès, 1, 08028 Barcelona, Catalunya, Spain
[c] Escuela de Física, Universidad Industrial de Santander, Carrera 27 calle 9 Ciudad Universitaria Bucaramanga, Colombia
[d] Department of Inorganic & Organic Chemistry, University of Barcelona, C/Martí i Franquès, 1, 08028 Barcelona, Catalunya, Spain
[e] Center of Materials and Nanotechnologies, Faculty of Chemical Technology, University of Pardubice, 53002, Czech Republic
[f] Central European Institute of Technology, Brno University of Technology, 61200, Czech Republic

ARTICLE INFO

Keywords:
Hydrogen evolution reaction
Molybdenum carbide
Graphene nanowalls
Graphene defects

ABSTRACT

To accelerate the transition to a green economy based on hydrogen, more efficient and cost-effective electrocatalysts should be adapted. Among them, transition metal carbides, particularly Mo_2C, have gained significant attention within the scientific community due to their abundance and potential for high performance in the hydrogen evolution reaction (HER). This study introduces a bottom-up approach involving chemical vapor deposition, impregnation in solvent containing the Mo precursor and thermal annealing processes to carburize the Mo nanostructures anchored on vertical graphene nanowalls supports (GNWs). The role of GNWs is highlighted in the above processes. First, they provide abundant defective sites on their edges, which facilitate the binding of the metal compound molecules. Second, they provide C species during the annealing process which migrate and react with the transition metal to carburize it. Thus, they act as both C precursor and support system. Electrochemical characterization shows that the hybrids can be very efficient electrocatalysts towards hydrogen evolution reaction in acid electrolyte. When used as a cathode in a cell, it requires only − 141 mV to generate 10 mA/cm^2 and shows excellent stability after hours of operation, making them highly promising for practical applications. This study paves the way for the design of hybrid nanostructures, utilizing nanocatalyst deposition on three-dimensional graphene supports. Such advancements hold great potential for driving the development of sustainable and efficient hydrogen production systems.

1. Introduction

The advancements in fuel cell technology have sparked optimism for the practical utilization of hydrogen as a promising energy carrier [1,2]. Among various hydrogen production methods, water electrolysis has garnered special interest. However, for this approach to be economically viable for large-scale applications, highly efficient electrocatalysts, particularly for the HER, are urgently needed. Although noble metals, especially Pt, have demonstrated outstanding catalytic performance, their high cost and limited availability hinder widespread commercial application [3–6]. Therefore, there is a pressing need to explore novel, cost effective, and easily accessible electrocatalysts.

Transition metal (TM)-based compounds are extensively studied for the above application, since they are more accessible and resistant against corrosion, an important feature regarding electrolysis in acidic mediums [7–15]. Transition metal carbides (TMCs), especially Mo_2C, in many cases are reported to approach the electrocatalytic activity of noble metals. The incorporation of carbon into the interstitial sites of the parent transition metal, as observed in Mo_2C, leads to a unique surface reactivity due to an increased metal–metal bond distance and a higher density of states near the Fermi level [16,17]. Experimental evidences have confirmed that Mo_2C is very promising catalyst for HER in acidic conditions [18,19]. Consequently, research efforts are recently focused on further enhancing this activity by development of nanostructures

* Corresponding author at: Department of Applied Physics, University of Barcelona, C/Martí i Franquès, 1, 08028 Barcelona, Catalunya, Spain.
E-mail address: stefanoschaitoglou@ub.edu (S. Chaitoglou).

https://doi.org/10.1016/j.jallcom.2023.172891
Received 15 September 2023; Received in revised form 3 November 2023; Accepted 16 November 2023
Available online 19 November 2023

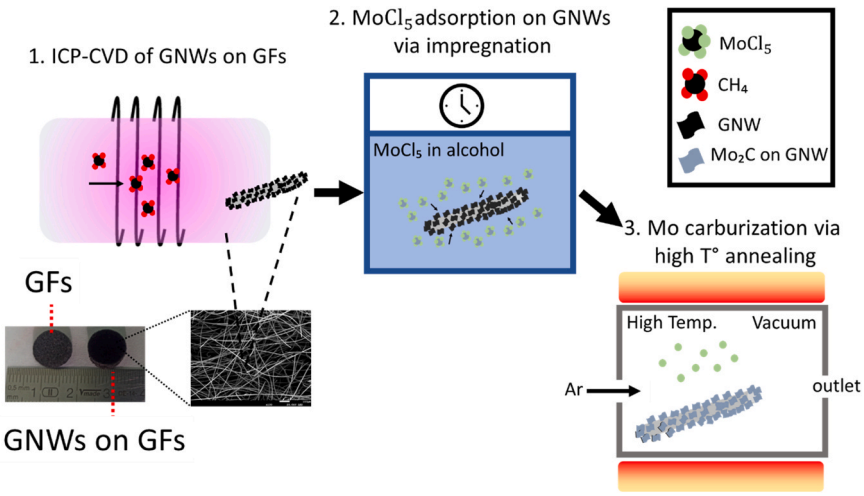

Fig. 1. Schematic illustration of the preparation steps to synthesize the Mo_2C on GNWs compounds. 1. ICP-CVD of GNWs on GFs. A digital image of the GFs before and after the GNWs deposition and a SEM image showing the interconnected structure formed by the graphite fibers. 2. Adsorption of $MoCl_5$ on GNWs through immersion in the $MoCl_5$/isopropanol solution. 3. High temperature annealing resulting in Cl evaporation and Mo carburization.

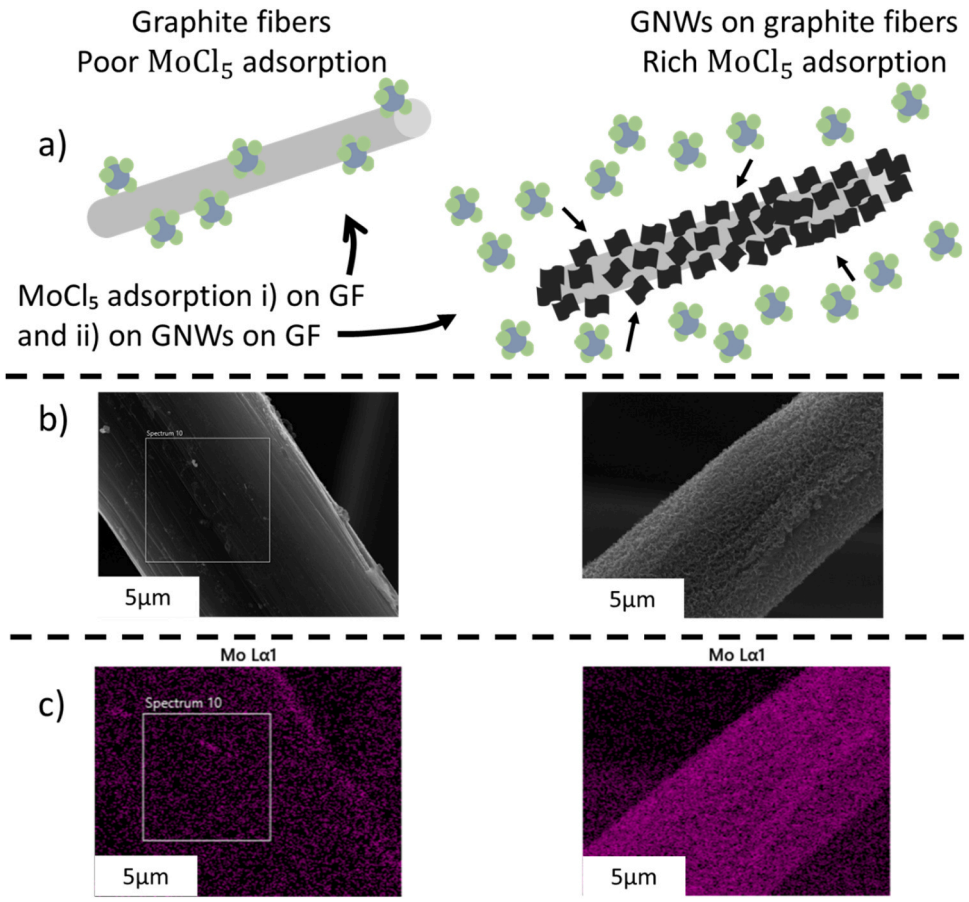

Fig. 2. a) illustration of $MoCl_5$ adsorption on GFs (left) and GNWs on GFs (right). b) SEM and c) Mo EDS map images of $MoCl_5$ adsorbed on GFs and (left) and GNWs on GFs (right). Scale bar is 5 μm.

with high active surface area, which offer an abundancy of active sites, and hybridization with other materials that can facilitate the relevant electrochemical reactions. In this context, carbon nanomaterials, especially graphene-based compounds, have been widely explored. Experimental results have shown that the conductivity of electrocatalysts increases upon hybridization with graphene-based materials, like graphene nanosheets [20,21] and carbon nanotubes [22]. For the case of Mo_2C, similar observations have been made when the compound is combined with graphene nanowalls (GNWs) [23]. Density functional theory calculations have confirmed that the introduction of Mo_2C onto graphene structures reduces the free energy barriers associated with the hydrogen HER mechanism. This reduction is achieved by promoting the adsorption of H* and facilitating the desorption of molecular hydrogen [24]. Therefore, the utilization of GNWs to synthesize hybrid

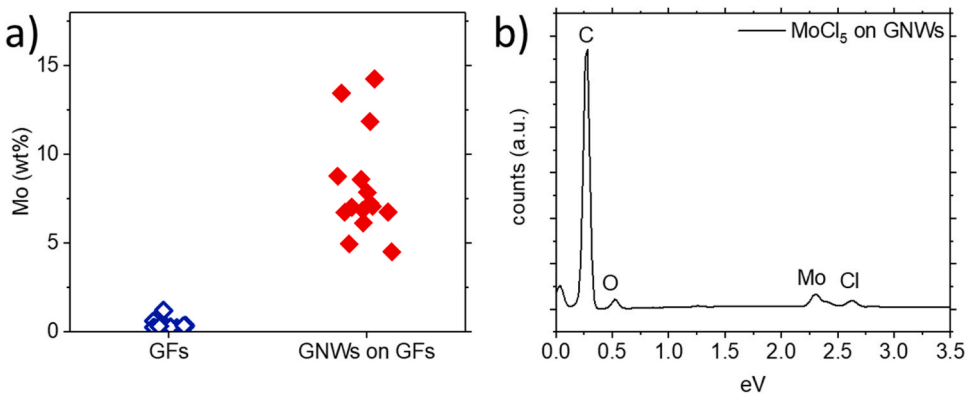

Fig. 3. a) %Wt of Mo content after $MoCl_5$ adsorption on GFs (blue points) and on GNWs on GFs (red points). b) EDS spectrum of GNWs on GFs after impregnation with $MoCl_5$.

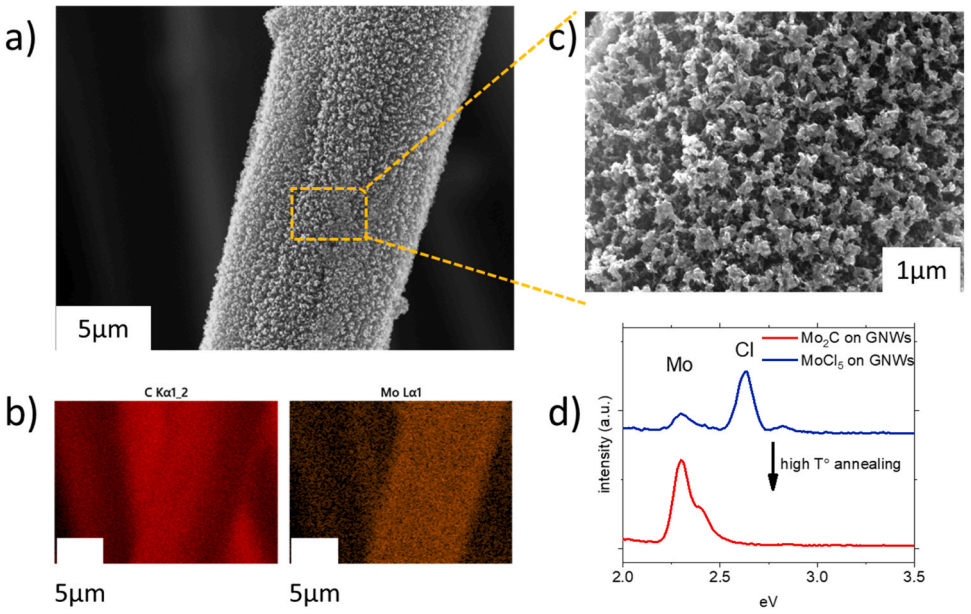

Fig. 4. a-b) SEM image of Mo_2C on GNWs on CFs and Mo and C EDS map, showing the homogeneous distribution of Mo on the fiber's surface. Scale bar is 5 μm c) zoomed SEM image of the GNWs surface, showing the formation of nanocrystalline Mo_2C particles on the GNWs. Scale bar is 1 μm. d) EDS spectra of sample before and after high temperature annealing, showing the absence of Cl.

compounds altogether with Mo_2C, can be highly beneficial, especially when considering the very high active surface area of this graphene allotrope. Previous studies have demonstrated a remarkable 6-fold increase in the capacitance of electrodes, when decorated with GNWs [25]. Furthermore, when Mo_2C particles were deposited on GNWs by means of magnetron sputtering of Mo and in-situ annealing and carburization, the hybrid compounds exhibited one of the highest recorded electrocatalytic activities for HER [21] for this class of materials.

This study presents a simple but efficient way to prepare Mo_2C/graphene hybrid compounds, through immersion of the GNWs deposited on graphite felt (GF) on a solution of $MoCl_5$ dispersed in isopropanol. $MoCl_5$ has been successfully used as Mo precursor for synthesis of Mo_2C on metal organic frameworks through high temperature carburization in a CH_4 atmosphere [26]. Its use is convenient since Cl species are easily evaporated at relatively low temperature and the remaining Mo can react with the introduced gas precursor to form the carbides. The role of GNWs is twofold. First, they possess a high number of structural defects, especially at their edges, facilitating the homogenous adsorption of $MoCl_5$ molecules [27], without requiring additional heating or other treatment. Secondly, during the subsequent annealing at high temperatures, carbon atoms from the GNWs migrate and react with Mo to form the desired carbides, eliminating the need for additional carbon precursor. Furthermore, the GNWs possess appealing intrinsic properties like high electrical conductivity and high surface to volume ratio, as well as very strong adhesion on the electrode substrate. The last feature is important regarding performance stability, especially when operating in high current densities and for long periods of time. A schematic illustration of the preparation process is provided in Fig. 1. The resulting nanostructures are tested as working electrodes for HER, demonstrating efficient activity and good durability.

2. Experimental part

2.1. Synthesis of GNWs on GFs

GNWs were deposited on commercial graphite felts (purchased by Mersen) by inductively coupled plasma-chemical vapor deposition (ICP-CVD). A detailed description of the synthesis process can be found in the literature [28]. Briefly, the deposition reactor was an ICP-CVD system (13.56 MHz, power = 440 W) comprising a long quartz tube, a radio frequency (RF) resonator for producing remote plasma, and a tubular oven. The GFs were cut in circular pieces of 1 cm in diameter. They were

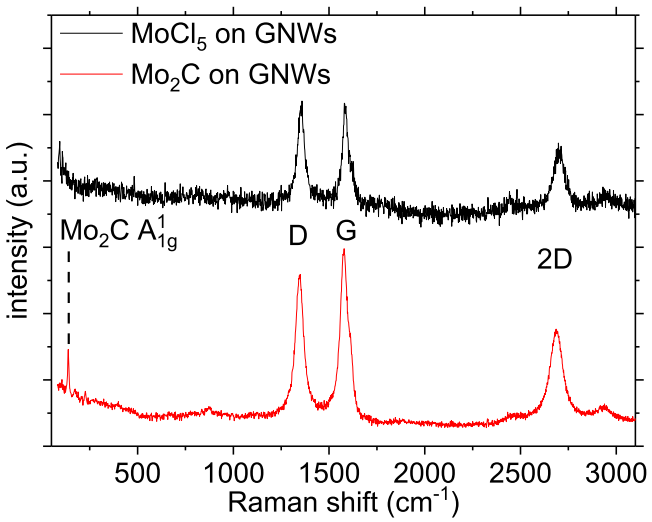

Fig. 5. Raman spectra of GNWs decorated with $MoCl_5$ particles, before (black spectrum) and after (red spectrum) high temperature annealing resulting in Mo carburization.

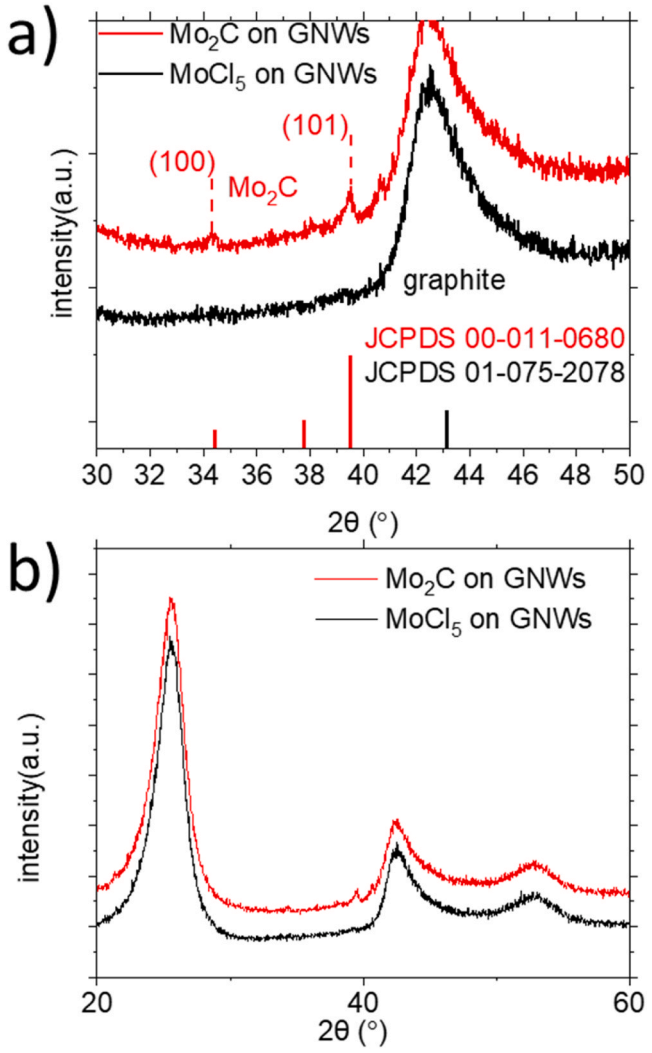

Fig. 6. a) XRD patterns of $MoCl_5$ adsorbed on GNWs deposited on GF (black spectrum) and Mo_2C on GNWs, formed upon the high temperature annealing treatment (red spectrum) (top of Fig.). JCPDS patterns of graphite and Mo_2C are visible on Fig. bottom. b) wide scan of the XRD patterns depicted in a).

cleaned with isopropanol and distilled water and dried before introduced in the reactor. The sample was positioned 30 cm away from the plasma zone and heated to a temperature of 750 °C while reducing the reactor pressure to approximately 10^{-4} mTorr using a turbomolecular pump. Initially, the surface of GFs was cleaned by subjecting it to H_2 plasma. This cleaning process involved applying an RF power of 400 W at a pressure of 400 mTorr of H_2 for 5 min. Subsequently, the H_2 flow was halted, and a CH_4 plasma was generated under the same RF power and pressure conditions to initiate the growth of graphene nanowalls (GNWs). The growth of GNWs took place for a duration of 30 min. The GNWs on the GFs sample were then allowed to cool down to room temperature (approximately 20 °C) under vacuum. Finally, a short-duration O_2 plasma treatment was administered to the GNW surface to enhance its hydrophilicity. This treatment involved applying an RF power of 40 W at a pressure of 400 mTorr for 30 s. Following the completion of the process, the GNWs on the GFs sample was removed from the reactor.

2.2. Deposition of Mo_2C

The GNWs on GFs sample was immersed in a solution containing 0.032 milligrams of $MoCl_5$ (purchased from Sigma Aldrich, purity of 95%) in 100 ml of isopropanol and let for 1 h, at room temperature. Then, they were removed and dried in a hot plate at 80 °C. The dried sample was introduced in a reactor used for chemical vapor deposition processes, which consists of a tubular oven and a quartz tube. The pressure of the reactor was decreased to ~10^{-3} mTorr using a turbomolecular pump. Then, the sample was heated up to 950 °C under argon atmosphere of 1 Pa, maintained by a constant flow of 10 sccm of Ar. Previous studies showed that the annealing in lower temperatures results in the synthesis of a Mo oxycarbide compound with poorer electrocatalytic activity [23]. The sample was annealed in this temperature for 10 min. The Mo compounds were carburized upon reaction with C originating by the GNWs through migration. Once the annealing was terminated, the sample was cooled in room temperature under argon atmosphere, before removed from the reactor for further characterization.

2.3. Physical characterization

The morphology of the Mo_2C on GNWs samples was examined using scanning electron microscopy (SEM) (JEOL JSM-7001 F, operated at 20 kV) and transmission electron microscopy (TEM) (JEOL 1010, operated at 200 kV). The elemental composition of the samples was obtained by energy-dispersive X-ray spectroscopy (EDS). For TEM observation, the nanostructures were transferred onto a Cu grid by applying pressure with a cotton stick to remove from the growth substrate. SEM and TEM images were processed using Image J and Digital Micrograph software. X-ray photoelectron spectroscopy (XPS) was performed using a PHI 5500 Multi-Technique System (Physical Electronics, Chanhassen, MN, USA) with a monochromatic X-ray source (Al Ka line of 1486.6 eV energy and 350 W) positioned perpendicular to the analyzer axis and calibrated using the Ag $3d_{5/2}$ line at a full-width half-maximum (FWHM) of 0.8 eV. The analyzed area was a circle with a diameter of 0.8 mm, and the selected resolution for the survey XPS spectra had a pass energy of 187.5 eV and 0.8 eV/step and the selected resolution for the elemental spectra had a pass energy of 11.75 eV and 0.1 eV/step. The vibrational modes of the Mo_2C on GNWs samples were studied using a Raman microscope (HR800, Lab-Ram; HORIBA France SAS, Palaiseau, France) with a 532-nm solid-state laser (laser power = 5 mW; diameter = ~1 μm). For X-ray diffraction (XRD) measurements, a PANalytical XPert PRO MPD Bragg-Brentano powder diffractometer with a 240-mm radius was used. Samples were exposed to Co Ka radiation (λ = 1.789 Å) in a 2θ range from 4° to 99° with a step size of 0.017° and a measuring time of 200 s per step.

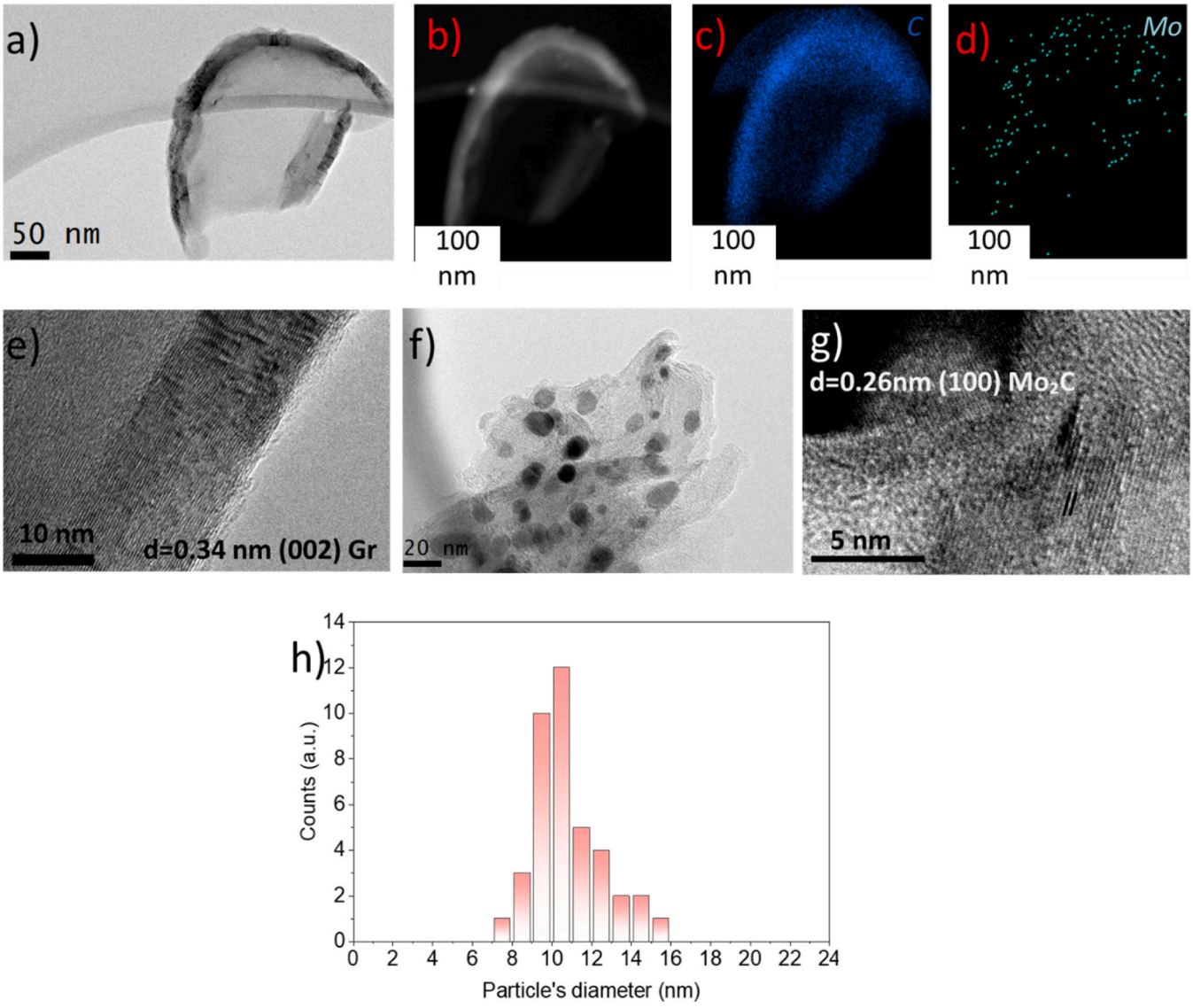

Fig. 7. Characterization of Mo_2C on GNWs by a) TEM image showing a GNW flake decorated with Mo_2C particles on its edges, b) backscattered electrons image of the same area, c-d) EDS maps of C and Mo present on the same area. e) TEM image of the GNWs edges depicting the graphene planes. f) TEM image showing the distribution of Mo_2C particles on the GNWs. g) HRTEM image depicting the Mo_2C planes. h) Size distribution histogram of the Mo_2C nanoparticles.

2.4. Electrochemical characterization

The electrochemical properties of the compounds were studied using a potentiostat/galvanostat (AutoLab, PGSTAT30, Eco Chemie B.V.). All experiments were performed at room temperature in a typical three-electrode cell. An Ag/AgCl electrode (an internal 3 M KCl solution) and a Pt electrode (purchased from Metrohm; the Pt tip was separated by porous glass to avoid dissolution into the electrolyte and sample contamination) were used as the reference and counter electrodes, respectively. The working electrode was nanostructured Mo_2C deposited on the GNWs on GFs or bare GFs support and was electrically connected to power supply via a crocodile clip. Linear sweep voltammetry (LSV) was performed with a scan rate of 5 mV s^{-1} in a 0.5 M H_2SO_4 electrolyte. The surface area of the electrodes was always 0.8 cm^2. LSV measurements were performed 10 times before recording the data to ensure stable performance of the electrode.

All potentials were converted against the RHE using the Nernst law equation as follows:

$$E_{RHE} = E_{Ag/AgCl} + 0.21 + 0.050x \quad pH$$

where E_{RHE} is the potential of the RHE and $E_{Ag/AgCl}$ is the measured potential against the Ag/AgCl (3 M KCl) reference electrode. Charge transfer resistance was measured via electrochemical impedance spectroscopy (EIS) in the frequency range from 100 kHz to 0.1 Hz. All electrodes were stored under ambient conditions and were characterized several days to weeks after electrode preparation. All electrochemical measurements were performed at room temperature.

3. Results and discussion

In this study, they are investigated the remarkable properties of Mo_2C deposited on GNWs and its potential as an efficient electrocatalyst for the HER. The synthesis and characterization of the Mo_2C-GNWs hybrid were conducted, and the obtained results are presented and discussed below.

Firstly, it is examined the morphology of the Mo_2C-GNWs hybrid using SEM (Fig. 2). Fig. 2b (left) shows an individual graphite fiber (GF), with a diameter of approximately 10 μm. On the right side of Fig. 2b, they are observed SEM images of GNWs deposited on the GF surface, forming a dense and homogeneous network. These samples were

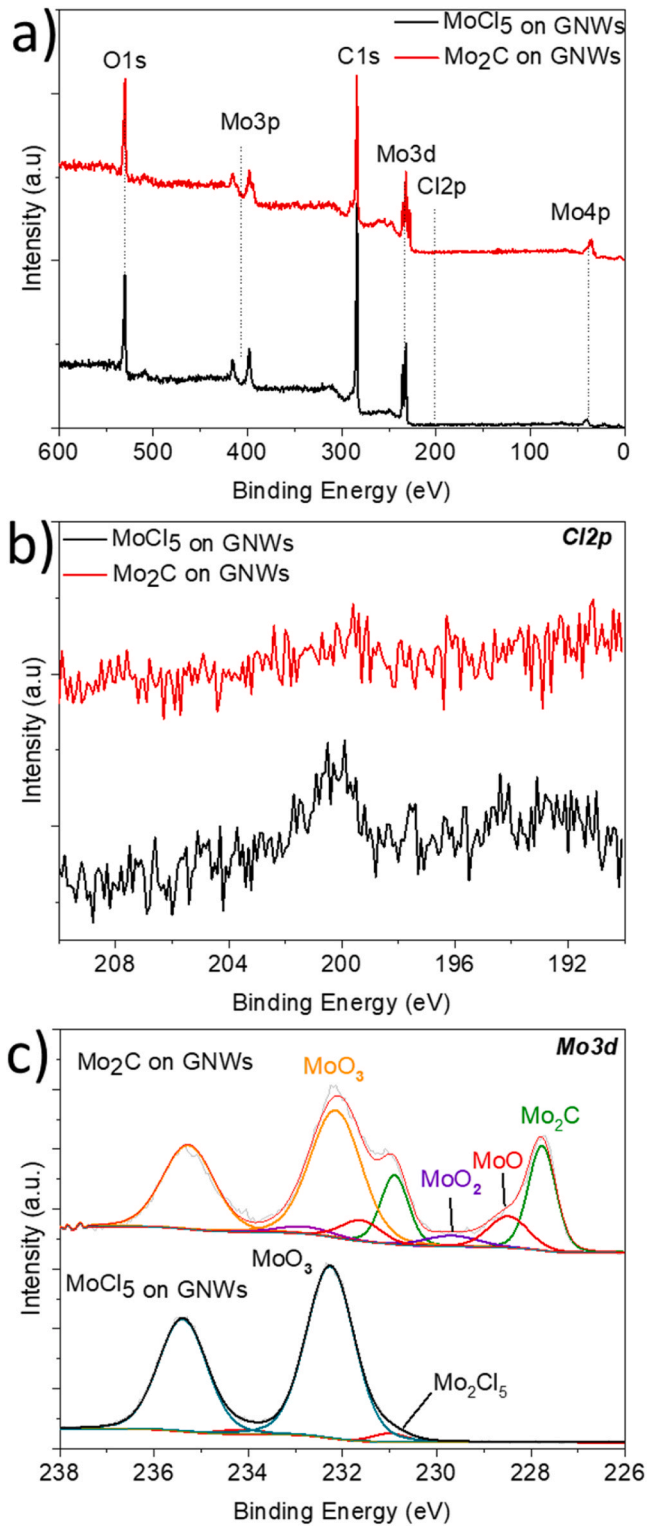

Fig. 8. a) Survey XPS spectra before (black graph) and after (red graph) annealing of the Mo on GNWs compounds. b) Cl 2p spectra before (black graph) and after (red graph) annealing of the Mo on GNWs compounds. c) Mo 3d spectra before (bottom graph) and after (top graph) annealing of the Mo on GNWs compounds.

immersed in a solution containing $MoCl_5$ in isopropanol to investigate the role of the GNWs as a support for the adhesion of $MoCl_5$ molecules. GNWs exhibit defective edges that favor the binding of the $MoCl_5$, leading to a higher concentration of $MoCl_5$ on the GNWs-GFs samples (Fig. 2a). The enhanced presence of edge defects on the GNWs has been reported before and is manifested in the Raman fingerprint of the compound and specifically on the evolution of the $FWHM_G$ with respect to the I_D/I_G [29]. This is further confirmed by Mo EDS mapping images (Fig. 2c), which show a more homogeneous deposition of Mo across the GNWs surface compared to the bare GFs. Quantification of the Mo content by EDS analysis reveals that the Mo wt% content is less than 1.2%, while on the GNWs-GFs surface, it varies between approximately 5–15% (Fig. 3a). Additionally, EDS detects Cl, C and O (Fig. 3b).

During high temperature annealing in Ar, Cl evaporates and C species originating from the GNWs migrate towards Mo and react to form the Mo carbide crystals. A SEM image of the resulting compounds shows the homogeneous coverage of the GNWs with Mo_2C crystals. This is confirmed by the EDS maps of Mo and C (Fig. 4a-b). Zoomed SEM image shows the formation of nanocrystalline Mo_2C deposited on the GNWs. These nanocrystals in the form of particles have sizes in the order of hundreds of nm in diameter (Fig. 4c). In addition, the comparison of compound's EDS spectrum before (blue spectrum) and upon (red spectrum) annealing shows the complete absence of Cl in the later, pointing that during evaporation it is eliminated from sample's surface (red spectrum) (Fig. 4d).

The Raman fingerprint of the GNWs provides information regarding the thickness in terms of number of layers and the density of defects in the crystal structure. The broadening of the 2D peak is a result of its splitting into four clustered peaks, oppositely to the presence of a single peak for the case of single layer graphene [29]. The FWHM of the 2D mode is 67 cm^{-1}, which reveals the presence of ~5 at. layers [28]. The density of defects can be calculated taking into consideration the intensity ratio between the D and G modes, $\frac{I_D}{I_G}$. Briefly, the defects' density can be calculated by the equation:

$$n_D\left(cm^{-2}\right) = \frac{(1.8 \pm 0.5)x10^{22}x(\frac{I_D}{I_G})}{\lambda_L^4},$$

where λ is the laser wavelength in nm [30,31]. For the as-synthesized GNWs, decorated with $MoCl_5$, this ratio is ~approximately 1 (Fig. 5, black spectrum). Upon annealing and Mo carburization, it is observed a reduction on the intensity of the D peak (Fig. 5, red spectrum). The resulting $\frac{I_D}{I_G}$ ratio is ~0.84. This implies a decrease on the defects' density upon annealing and points towards the hypothesis that C species anchored on defective sites on GNWs migrate and carburize Mo particles during annealing. The C atoms forming the graphene lattice re-organize themselves and a less defective graphene crystal structure results through this re-crystallization process. A similar trend has been observed in past studies during the carburization of sputtered Mo film deposited on GNWs [23]. In addition, after the annealing a new band appears at ~143 cm^{-1}, which is attributed to the formation of the orthorhombic phase of Mo_2C [32].

Fig. 6a illustrates the XRD patterns of the $MoCl_5$ deposited on the GNWs before and after the annealing process. Before annealing, the observed diffraction peaks are attributed to the GNWs on the graphite felt substrate, since the adsorbed $MoCl_5$ do not generate any signal (black spectrum). Thus, three bands attributed to graphite are detected at 25.6°, 42.6° and 52.8° (Fig. 6b). They are attributed to the graphite felt and indicate its polycrystalline nature. It is known that GNWs exhibit a diffraction peak at 30.35°, which in the present case is not observed because it coincides with the shoulder signal of the graphite peak [25]. After annealing, additional peaks appear at 34.3° and 39.5°, attributed to the (100) and (101) planes of orthorhombic Mo_2C (red spectrum). Thus, XRD analysis agrees with the findings of Raman spectroscopy analysis and confirms the formation of crystalline Mo_2C particles in the GNWs surface. At bottom of Fig. 6a are exhibited the position and intensity of the diffraction peaks of graphite and orthorhombic Mo_2C, as these are obtained from the respective JCPDS patterns.

TEM characterization results are depicted in Fig. 7. Fig. 7a-b show a GNW flake in transmission and backscattered electrons modes

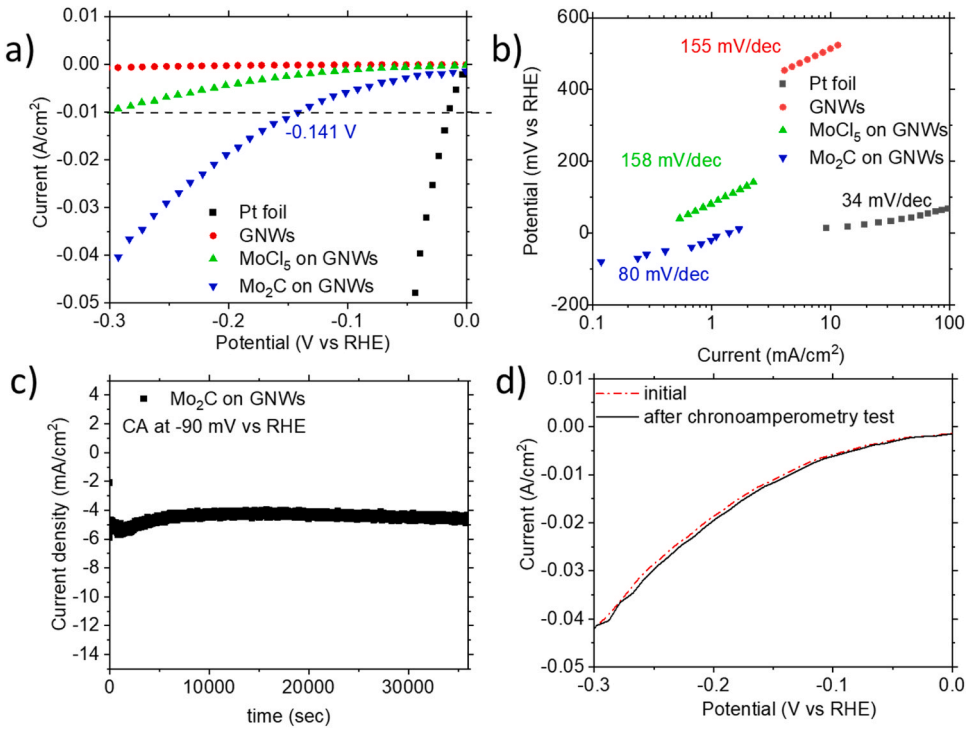

Fig. 9. a) LSV curves of GNWs (red curve), $MoCl_5$ on GNWs (green curve), Mo_2C on GNWs (blue curve) and Pt foil (black curve). b) Tafel slopes of the same materials. Depicted with the same colors. c) chronoamperometry test of the Mo_2C on GNWs electrode during 10 h. d) LSV curves comparison before and after the chronoamperometry test described in c).

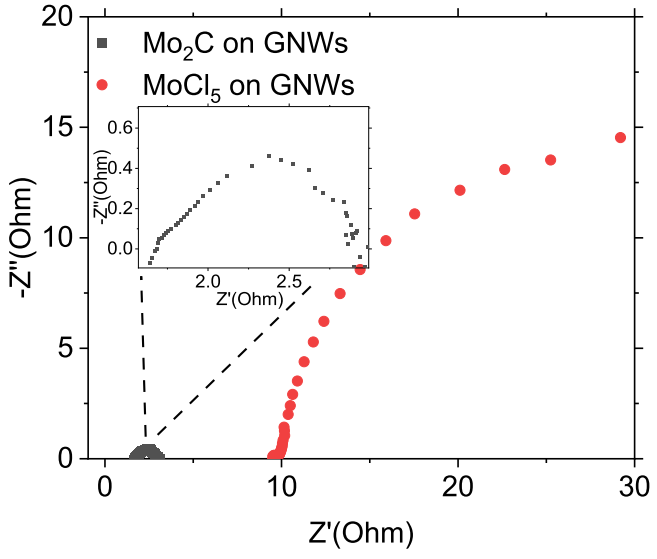

Fig. 10. Nyquist plots of the as-deposited $MoCl_5$ on GNWs (red graph) and the final Mo_2C on GNWs (black graph), resulting upon annealing.

respectively. It can be appreciated the deposition of the Mo_2C particles in the edges of the GNWs. This observation is of particular interest, since it proves that $MoCl_5$ molecules are favorably adsorbed on the defective edges and not on the basal plane of the GNWs. Fig. 7c-d show elemental maps of C and Mo respectively, as acquired by EDS. It can be especially appreciated the presence of Mo on the edges of the GNW flake. Moreover, C signal is stronger in these areas, since C present in Mo_2C contributes to the signal enhancement. Fig. 7e shows a high-resolution TEM image of the edge of the GNW flake. Fast Fourier transform in the area where the graphite planes are visible confirms a lattice distance of 0.34 nm, corresponding to the (002) orientation of graphene. Fig. 7f shows various Mo_2C particles deposited on the GNWs framework. High-resolution image of these particles reveals lattice fringes with a 0.26 nm distance, corresponding to the (100) orientation of orthorhombic Mo_2C (Fig. 7g), which lies in agreement with the observations made by XRD characterization shown above. The size distribution histogram of the particles is presented in Fig. 7h. The particles diameter varies between 7 and 16 nm. Most common values lie between 9 and 11 nm. XPS measurements are made to characterize the surface states of the Mo compounds on GNWs. Survey spectra of the $MoCl_5$ on GNWs before (black spectrum) and after (red spectrum) annealing are shown in Fig. 8a. All peaks are assigned to signals from C, Mo, and O, confirming the absence of any surface contamination on the Mo_2C on GNWs. Importantly, the absence of Cl signals in the XPS spectra confirms the complete evaporation of Cl species during annealing. The Cl 2p peak of the sample before and after carburization are exposed in Fig. 8b. The as-deposited $MoCl_5$ shows a Cl 2p peak centered at 200.2 eV (red curve). It can be observed that upon carburization no Cl signal is detected (black curve), proving the sufficient evaporation of the Cl species. The Mo 3d peak is depicted in Fig. 8c. Before carburization, main peaks are centered at 232.2 eV and 235.4 eV, attributed to MoO_3 species [33]. Additional weak peaks attributed to $MoCl_5$ are located at 231 eV and 234.1 eV (bottom graph). After carburization, new peaks arise at 229.7 eV and 232.9 eV, attributed to MoO_2, as well as at 228.5 eV and 23.7 eV, attributed at MoO. Peaks attributed at Mo_2C arise at 227.8 eV and 230.9 eV (top graph) [34]. The presence of oxide peaks on the carburized compounds are attributed to inevitable surface oxidation upon exposure to atmosphere. This is supported by XRD and Raman spectroscopy characterization, where only the carbide phase is detected. The few atomic layers of oxide are considered as chemically transparent towards the electrochemical reaction and do not deteriorate the catalytic efficiency of the carbide structures [26,34]. Conclusively, XPS characterization confirms the carburization of Mo and formation of Mo_2C, which results from the evaporation of Cl species and migration of C species from the GNWs towards the Mo during the annealing step.

The electrocatalytic properties of Mo_2C on GNWs nanostructures

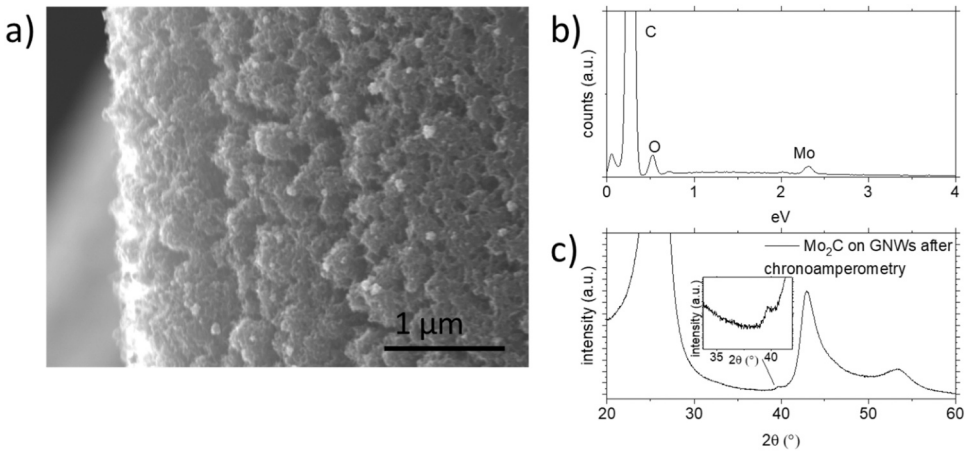

Fig. 11. Electrode characterization after chronoamperometry measurement: a) SEM image, b) EDS graph and c) XRD graph of the Mo_2C on GNWs compound after 1 h of chronoamperometry test. An image of the magnified area showing the diffraction peak of Mo_2C is placed as an inset.

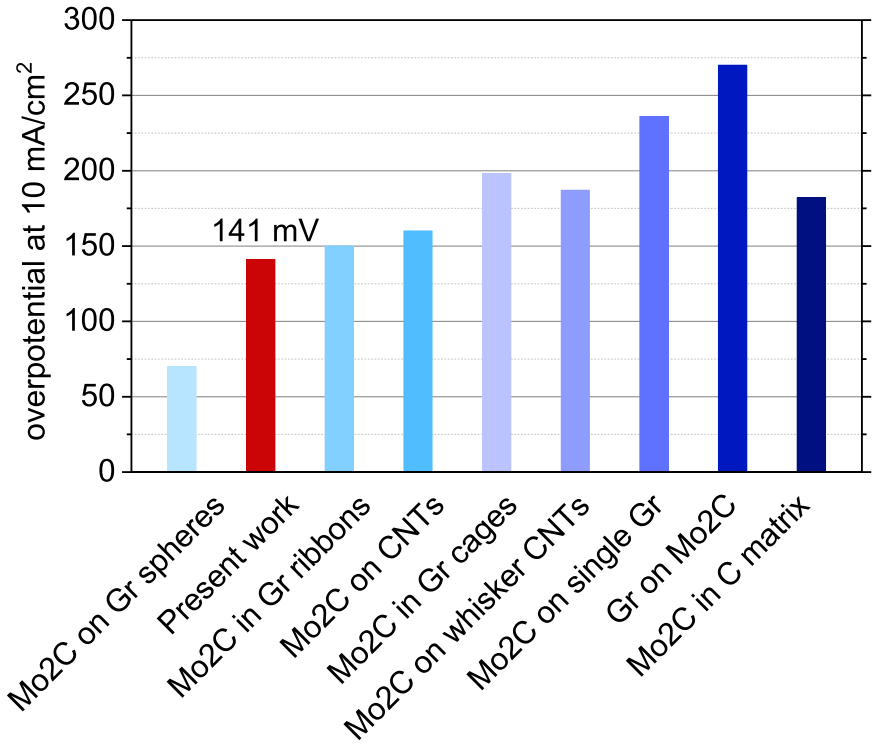

Fig. 12. Comparison of overpotential values required to produce 10 mA/cm^2 in acidic medium for various Mo_2C on carbon compounds.

toward the HER were evaluated by LSV. Results presented in Fig. 9a show the current density produced in the − 0.3–0 V range. Bare GNWs on GFs require higher onset potential for the HER to occur, thus there is no increase in current density (red curve) in the examined range. Similar poor activity is recorded for the as-adsorbed $MoCl_5$ on GNWs, which requires a relatively high overpotential of − 0.3 V for generation of 10 mA/cm^2 (green curve). This may be also due to the instability of $MoCl_5$ when dissolved in water [35]. Upon carburization, the Mo_2C on GNWs compounds require an overpotential of − 0.141 V for generation of 10 mA/cm^2 (blue curve). As expected, Pt foil electrocatalyst still showed the best performance, since it requires 0 onset potential and ~ approximately − 0.02 V to generate 10 mA/cm^2 (black curve). Moreover, the Tafel plots, presented in Fig. 9b, showed a fairly low Tafel slope of 80 mV per decade for Mo_2C on GNWs, higher than 34 mV per decade for the Pt foil but lower than 155 and 158 mV per decade that showed the GNWs and $MoCl_5$ on GNWs respectively. The relatively low Tafel slope of the Mo_2C on GNWs further suggests that the Volmer–Heyrovsky mechanism was the most operative in the HER reaction, thus the electrochemical desorption is the rate determining step [36]. Fig. 9c illustrates the variation of current density over time under a stable potential of − 90 mV, which generates ~5 mA/cm^2. It can be observed that there was only a negligible decrease in current density after 10 h, indicating the remarkable stability of Mo_2C on GNWs under the experimental conditions. Moreover, after 10 h of the chronoamperometry test, the LSV measurement was repeated. Fig. 9d illustrates the comparative polarization curves obtained before and after the chronoamperometry test. It was observed that the overvoltage required to achieve a current density of 10 mA/cm^2 remains unchanged. EIS measurements were performed to extract the charge-transfer characteristics of the $MoCl_5$ and Mo_2C compounds deposited on the GNWs. The results are presented in a Nyquist plot in Fig. 10. It is observed a dramatic drop in both the charge-transfer and series resistances upon the carburization process.

Specifically, the charge-transfer resistance value is reduced from 40 ohm for the $MoCl_5$ on GNWs, to only 1.3 Ohm for the Mo_2C on GNWs. Similarly, the series resistance is reduced from 10 Ohm for the $MoCl_5$ on GNWs, to only 1.6 Ohm for the Mo_2C on GNWs. The resistance drop is considered as an important factor which explains the superior electrocatalytic performance of the Mo_2C compounds. The structural and morphological stability of the compound after the chronoamperometry test is showcased in Fig. 11. Fig. 11a shows the SEM image of the nanostructure. The GNWs features can be distinguished, demonstrating their morphological stability. Fig. 11b shows the EDS graph of the compound after the chronoamperometry test. It can be observed the presence of Mo, C and O. No other elements are detected, proving that no contamination of the working electrode occurs during the test. Fig. 11c shows the wide scan of the diffraction peaks of the compound after the chronoamperometry test. The graphite peaks are not modified compared to the pristine sample (Fig. 6b). The Mo_2C (101) peak is observed at 39.5°, confirming the long-term structural stability of the compound in harsh acidic conditions. No oxide peaks are not apparent. The inset Fig. shows a magnification of the area where the Mo_2C peak is centered. In order to highlight the exceptional electrocatalytic properties of the hybrid Mo_2C on GNWs electrodes, they are compared the overpotential values ($j = 10\ mA/cm^2$) of various nanostructured Mo_2C-graphene compounds. These compounds demonstrate superior characteristics compared to most previously reported catalysts consisting of molybdenum carbide and graphene in 0.5 M H_2SO_4. For instance, the overpotential values for graphene on carburized Mo foil were $\eta_{10} = 270$ mV, for graphene on 2D Mo_2C were $\eta_{10} = 236$ mV, for Mo_2C in carbon cages were $\eta_{10} = 198$ mV, for Mo_2C on whisker carbon nanotubes (W-CNTs) were $\eta_{10} = 187$ mV, for Mo_2C in carbon matrix were $\eta_{10} = 182$ mV, for Mo_2C on CNTs were $\eta_{10} = 160$ mV, and for Mo_2C on graphene ribbons were $\eta_{10} = 150$ mV. Thus, the present values are surpassed only by Mo_2C in graphene microspheres, as shown in Fig. 12 [37–44]. The reduced charge transfer resistance of the present Mo_2C on GNWs compounds, combined with the presence of abundant active sites, have been showcased as the main reasons behind the superior electrocatalytic performance. Nevertheless, microscopy characterization showed that Mo_2C particles are favorably anchored on the defective edges of the graphene flakes (Fig. 7a). To further improve the HER activity, enhanced catalyst loading could be achieved by deposition on both the edges and basal plane of the support system. This can result in a higher number of available active sites and better overall activity. Various articles have recently reported the use of GNWs-based hybrid systems for use in energy storage and catalysis [23,45,46]. The present study aims in contributing insights towards the more efficient preparation of such advanced systems.

4. Conclusions

The present study reports a facile approach to prepare nanostructured Mo_2C crystals on GNWs supported on GFs. The unique lattice structure of the GNWs, combined with the formation of Mo_2C crystals, contributes to the improved electrochemical properties. The role of the GNWs here is dual, since they act as both a support system with a very high specific surface area and a carbon precursor for the carburization of Mo during high temperature annealing. The crystal defects present on the graphene lattice facilitate the enhanced anchoring of $MoCl_5$ precursor molecules, as quantified by EDS measurements. Microscopy characterization reveals that Mo_2C particles are preferentially bound on the defective edges of the graphene nanostructure. The resulting compounds are tested as catalyst electrodes towards hydrogen evolution reaction. They require just 141 mV for the generation of 10 mA/cm^2, a value that exceeds the performance of most Mo_2C/ graphene hybrids found in literature up today. The relatively low Tafel slope suggests that the Volmer-Heyrovsky mechanism dominates the reaction pathway, favouring the electrochemical desorption process and ultimately leading to the generation of hydrogen with reduced overpotential. The remarkable stability of the Mo_2C on GNWs hybrid under the experimental conditions adds further appeal to its potential application as an efficient and durable electrocatalyst. The negligible decrease in current density after prolonged operation indicates that the hybrid material maintains its catalytic activity over extended periods. The combination of Mo_2C with GNWs leads to a compelling enhancement in catalytic performance, making it a promising candidate for future clean energy technologies. These results are expected to provide useful insights regarding the preparation of TMCs/ graphene hybrids and the understanding of graphene's role in facilitating electrocatalytic reactions.

CRediT authorship contribution statement

Stefanos Chaitoglou: Conceptualization, Investigation, Methodology, Writing – original draft, Writing – review & editing. **Rogelio Ospina:** Investigation, Data curation. **Yang Ma**: Investigation, Methodology. **Roger Amade:** Funding acquisition, Supervision. **Xavier Vendrell:** Conceptualization, Funding acquisition, Supervision. **Jhonatan Rodriguez-Pereira:** Investigation. **Enric Bertran-Serra:** Funding acquisition, Supervision, Writing – original draft.

Declaration of Competing Interest

The authors declare the following financial interests/personal relationships which may be considered as potential competing interests: Stefanos Chaitoglou reports financial support was provided by European Commission.

Data availability

Data will be made available on request.

Acknowledgments

The publication of this article is funded by Grants PID2020-116612RB-C32 and TED2021-132070B-C21 provided by MCIN/AEI/10.13039/501100011033, in conjunction with financial support from the European Union. The ENPHOCAMAT group acknowledges support from the AGAUR of Generalitat de Catalunya, Project No. 2021SGR00936. S. C. and X. V. are thankful for the financial support from IN2UB through the Multidisciplinary Research Grant (ART_2022_1). Y.M. acknowledges the support from the predoctoral fellowship program funded by the China Scholarship Council affiliated with the Ministry of Education of the P. R China. S. C. acknowledges support from the postdoctoral fellowship programme Beatriu de Pinós, funded by the Secretary of Universities and Research (Government of Catalonia) through grant agreement 801370 (H2020-MSCA-COFUND-2017) and from the MSCA fellowship funded by the European Commission through grant agreement 101062014 (HORIZON Europe-MSCA-2021-PF-01). X.V. is a Serra Húnter Lecturer fellow and is grateful to the Generalitat de Catalunya. X. V. acknowledges the financial support from the Spanish Ministerio de Ciencia e Innovación (PID2020-116031RB-I00). R. O. acknowledges support from the postdoctoral fellowship programme María Zambrano, financed by the European Union and the Spanish Ministry for Science and Innovation.

Author contributions

The manuscript was written through the contributions of all authors. All authors have given approval to the final version of the manuscript.

References

[1] V.R. Stamenkovic, D. Strmcnik, P.P. Lopes, N.M. Markovic, Energy and fuels from electrochemical interfaces, Nat. Mater. 16 (2017) 57–69, https://doi.org/10.1038/nmat4738.

[2] Z.W. Seh, J. Kibsgaard, C.F. Dickens, I. Chorkendorff, J.K. Nørskov, T.F. Jaramillo, Combining theory and experiment in electrocatalysis: insights into materials design, Science 355 (2017) eaad4998, https://doi.org/10.1126/science.aad4998.

[3] Z. Wu, Pe Yang, Q. Li, W. Xiao, Z. Li, G. Xu, F. Liu, B. Jia, T. Ma, S. Feng, L. Wang, Microwave synthesis of Pt Clusters on black TiO_2 with abundant oxygen vacancies for efficient acidic electrocatalytic hydrogen evolution, Angew. Chem. Int. Ed. 62 (2023), e202300406, https://doi.org/10.1002/anie.202300406.

[4] Z. Chen, Q. Li, H. Xiang, Y. Wang, P. Yang, C. Dai, H. Zhang, W. Xiao, Z. Wu, L. Wang, Hierarchical porous NiFe-P@NC as an efficient electrocatalyst for alkaline hydrogen production and seawater electrolysis at high current density, Inorg. Chem. Front. 10 (2023) 1493–1500, https://doi.org/10.1039/D2QI02703H.

[5] M. Song, Z. Zhang, Q. Li, W. Jin, Z. Wu, G. Fu, Xien Liu, Ni-foam supported Co(OH)F and Co–P nanoarrays for energy-efficient hydrogen production via urea electrolysis, J. Mater. Chem. A 7 (2019) 3697–3703, https://doi.org/10.1039/C8TA10985K.

[6] Z. Wu, D. Nie, M. Song, T. Jiao, G. Fu, X. Liu, Facile synthesis of Co–Fe–B–P nanochains as an efficient bifunctional electrocatalyst for overall water-splitting, Nanoscale 11 (2019) 7506–7512, https://doi.org/10.1039/C9NR01794A.

[7] Y. Zhang, B. Zhang, Z. Yin, X. Ma, Y. Zhou, Bimetallic Ni–Mo nitride@N-doped C as highly active and stable bifunctional electrocatalysts for full water splitting, New J. Chem. 46 (2022) 11893–11901, https://doi.org/10.1039/D2NJ01303G.

[8] F. Yu, H. Zhou, Y. Huang, J. Sun, F. Qin, J. Bao, W.A. Goddard, S. Chen, Z. Ren, High-performance bifunctional porous non-noble metal phosphide catalyst for overall water splitting, Nat. Commun. 9 (2018), 2551, https://doi.org/10.1038/s41467-018-04746-z.

[9] Q. Gao, W. Zhang, Z. Shi, L. Yang, Y. Tang, Structural design and electronic modulation of transition-metal-carbide electrocatalysts toward efficient hydrogen evolution, Adv. Mater. 31 (2019), 1802880, https://doi.org/10.1002/adma.201802880.

[10] L. He, W. Zhang, Q. Mo, W. Huang, L. Yang, Q. Gao, Molybdenum carbide-oxide heterostructures: in situ surface reconfiguration toward efficient electrocatalytic hydrogen evolution, Angew. Chem. Int. Ed. 59 (2020) 3544–3548, https://doi.org/10.1002/anie.201914752.

[11] H. Lu, B. Gao, H. Zhang, X. Fan, L. Zheng, J. Tan, S. Wang, Y. Zhang, Q. Gao, Y. Tang, Self-supporting composited electrocatalysts of ultrafine Mo_2C on 3D-hierarchical porous carbon monoliths for efficient hydrogen evolution, J. Mater. Chem. A 8 (2020) 23265, https://doi.org/10.1039/d0ta06438f.

[12] X. Fan, C. Liu, M. Wu, B. Gao, L. Zheng, Y. Zhang, H. Zhang, Q. Gao, X. Cao, Y. Tang, Synergistic effect of dual active sites over Ru/α-MoC for accelerating alkaline hydrogen evolution reaction, Appl. Catal. B Environ. 318 (2022), 121867, https://doi.org/10.1016/j.apcatb.2022.121867.

[13] L. Ji, J. Wang, L. Guo, Z. Chen, In situ O_2-emission assisted synthesis of molybdenum carbide nanomaterials as an efficient electrocatalyst for hydrogen production in both acidic and alkaline media, J. Mater. Chem. A 5 (2017) 5178–5186, https://doi.org/10.1039/C6TA10145C.

[14] L. Ji, J. Wang, X. Teng, H. Dong, X. He, Z. Chen, N,P-doped molybdenum carbide nanofibers for efficient hydrogen production, ACS Appl. Mater. Interfaces 10 (17) (2018), https://doi.org/10.1021/acsami.8b00363.

[15] B. Qin, C. He, Y. Wei, L. Ji, T. Wang, Z. Chen, S. Wang, Interfacial engineering of heterostructured Mo_2C-Ru nanoparticles dispersed on 3D interconnected carbon nanobelts for highly efficient hydrogen evolution, Electrochim. Acta 444 (2023), 141977, https://doi.org/10.1016/j.electacta.2023.141977.

[16] J.G. Chen, Carbide and nitride overlayers on early transition metal surfaces: preparation, characterization, and reactivities, Chem. Rev. 96 (1996) 1477–1498, https://doi.org/10.1021/cr950232u.

[17] J.R. Kitchin, J.K. Nørskov, M.A. Barteau, J.G. Chen, Trends in the chemical properties of early transition metal carbide surfaces: a density functional study, Catal. Today 105 (2005) 66–73, https://doi.org/10.1016/j.cattod.2005.04.008.

[18] X. Zhang, C. Shi, B. Chen, A.N. Kuhn, D. Ma, H. Yang, Progress in hydrogen production over transition metal carbide catalysts: challenges and opportunities, Curr. Opin. Chem. Eng. 20 (2018) 68–77, https://doi.org/10.1016/j.coche.2018.02.010.

[19] S. Chaitoglou, T. Giannakopoulou, D. Tsoutsou, A. Vavouliotis, C. Trapalis, A. Dimoulas, Direct versus reverse vertical two-dimensional Mo_2C/graphene heterostructures for enhanced hydrogen evolution reaction electrocatalysis, Nanotechnology 30 (2019), 415404, https://doi.org/10.1088/1361-6528/ab3155.

[20] S. Chaitoglou, T. Giannakopoulou, T. Speliotis, A. Vavouliotis, C. Trapalis, A. Dimoulas, Mo_2C/graphene heterostructures: low temperature chemical vapor deposition on liquid bimetallic Sn–Cu and hydrogen evolution reaction electrocatalytic properties, Nanotechnology 30 (2019), 125401, https://doi.org/10.1088/1361-6528/aaf9e8.

[21] H. Wang, X. Wang, D. Yang, B. Zheng, Y. Chen, $Co_{0.85}Se$ hollow nanospheres anchored on N-doped graphene nanosheets as highly efficient, nonprecious electrocatalyst for hydrogen evolution reaction in both acid and alkaline media, J. Power Sources 400 (2018) 232–241, https://doi.org/10.1016/j.jpowsour.2018.08.027.

[22] R. Bose, B. Patil, V. Rajendiran Jothi, T.-H. Kim, P. Arunkumar, H. Ahn, S.C. Yi, Co_3Se_4 nanosheets embedded on N-CNT as an efficient electroactive material for hydrogen evolution and supercapacitor applications, J. Ind. Eng. Chem. 65 (2018) 62–71, https://doi.org/10.1016/j.jiec.2018.04.013.

[23] S. Chaitoglou, R. Amade, R. Ospina, E. Bertran-Serra, Hybrid nanostructured compounds of Mo_2C on vertical graphene nanoflakes for a highly efficient hydrogen evolution reaction, ACS Appl. Energy Mater. 6 (2023) 6120–6131, https://doi.org/10.1021/acsaem.3c00625.

[24] D.C. Tranca, F. Rodríguez-Hernández, G. Seifert, X. Zhuang, Theoretical models for hydrogen evolution reaction at combined Mo_2C and N – doped graphene, J. Catal. 381 (2020) 234–247, https://doi.org/10.1016/j.jcat.2019.10.028.

[25] S. Chaitoglou, R. Amade, E. Bertran, Insights into the inherent properties of vertical graphene flakes towards hydrogen evolution reaction, Appl. Surf. Sci. 592 (2022), 153327, https://doi.org/10.1016/j.apsusc.2022.153327.

[26] M. Qamar, A. Adam, B. Merzougui, A. Helal, O. Abdulhamid, M.N. Siddiqui, Metal–organic framework-guided growth of Mo_2C embedded in mesoporous carbon as a high-performance and stable electrocatalyst for the hydrogen evolution reaction, J. Mater. Chem. A 4 (2016) 16225–16232, https://doi.org/10.1039/C6TA06553H.

[27] M.D. Bhatt, H. Kim, G. Kim, Various defects in graphene: a review, RSC Adv. 12 (2022) 21520–21547, https://doi.org/10.1039/D2RA01436J.

[28] E. Bertran-Serra, A. Musheghyan-Avetisyan, S. Chaitoglou, R. Amade-Rovira, I. Alshaikh, F. Pantoja-Suárez, J.-L. Andújar-Bella, T. Jawhari, A. Perez-del-Pino, E. Gyorgy, Temperature-modulated synthesis of vertically oriented atomic bilayer graphene nanowalls grown on stainless steel by inductively coupled plasma chemical vapour deposition, Appl. Surf. Sci. 610 (2023), 155530, https://doi.org/10.1016/j.apsusc.2022.155530.

[29] Y. Hao, Y. Wang, L. Wang, Z. Ni, Z. Wang, R. Wang, C.K. Koo, Z. Shen, J.T. L. Thong, Probing layer number and stacking order of few-layer graphene by Raman spectroscopy, Small 6 (2010) 195–200, https://doi.org/10.1002/smll.200901173.

[30] L.G. Cançado, A. Jorio, E.H.M. Ferreira, F. Stavale, C.A. Achete, R.B. Capaz, M.V. O. Moutinho, A. Lombardo, T.S. Kulmala, A.C. Ferrari, Quantifying Defects in Graphene via Raman Spectroscopy at Different Excitation Energies, Nano Lett. 11 (2011) 3190–3196, https://doi.org/10.1021/nl201432g.

[31] S. Chaitoglou, E. Bertran, Control of the strain in chemical vapor deposition-grown graphene over copper via H_2 flow, J. Phys. Chem. C 120 (2016) 25572–25577, https://doi.org/10.1021/acs.jpcc.6b07055.

[32] S. Chaitoglou, P. Tsipas, T. Speliotis, G. Kordas, A. Vavouliotis, A. Dimoulas, Insight and control of the chemical vapor deposition growth parameters and morphological characteristics of graphene/Mo_2C heterostructures over liquid catalyst, J. Cryst. Growth 495 (2018) 46–53, https://doi.org/10.1016/j.jcrysgro.2018.05.015.

[33] N.S. McIntyre, D.D. Johnston, L.L. Coatsworth, R.D. Davidson, J.R. Brown, X-ray photoelectron spectroscopic studies of thin film oxides of cobalt and molybdenum, Surf. Interface Anal. 15 (1990) 265–272, https://doi.org/10.1002/sia.740150406.

[34] J. Li, C. Zhou, J. Mu, E.-C. Yang, X.-J. Zhao, In situ synthesis of molybdenum carbide/N-doped carbon hybrids as an efficient hydrogen-evolution electrocatalyst, RSC Adv. 8 (2018) 17202–17208, https://doi.org/10.1039/C8RA02020E.

[35] M. Inagaki, G. Watanabe, Stability of $MoC1_5$-GICs in various solutions, Synth. Met. 94 (1998) 235–238, https://doi.org/10.1016/S0379-6779(98)00020-4.

[36] F. Bao, E. Kemppainen, I. Dorbandt, R. Bors, F. Xi, R. Schlatmann, R. van de Krol, S. Calnan, Understanding the hydrogen evolution reaction kinetics of electrodeposited nickel-molybdenum in acidic, near-neutral, and alkaline conditions, ChemElectroChem 8 (2021) 195–208, https://doi.org/10.1002/celc.202001436.

[37] S. Chaitoglou, T. Giannakopoulou, G. Papanastasiou, D. Tsoutsou, A. Vavouliotis, C. Trapalis, A. Dimoulas, Cu vapor-assisted formation of nanostructured Mo_2C electrocatalysts via direct chemical conversion of Mo surface for efficient hydrogen evolution reaction applications, Appl. Surf. Sci. 510 (2020), 145516, https://doi.org/10.1016/j.apsusc.2020.145516.

[38] D. Geng, X. Zhao, Z. Chen, W. Sun, W. Fu, J. Chen, W. Liu, W. Zhou, K.P. Loh, Direct synthesis of large-area 2D Mo_2C on in situ growth graphene, Adv. Mater. 29 (2017) 1700072.

[39] M. Qiang, X. Zhang, H. Song, C. Pi, X. Wang, B. Gao, Y. Zheng, X. Peng, P.K. Chu, K. Huo, General synthesis of nanostructured Mo_2C electrocatalysts using a carbon template for electrocatalytic applications, Carbon 197 (2022) 238–245, https://doi.org/10.1016/j.carbon.2022.06.016.

[40] S. Wu, M. Chen, W. Wang, J. Zhou, X. Tang, D. Zhou, C. Liu, Molybdenum carbide nanoparticles assembling in diverse heteroatoms doped carbon matrix as efficient hydrogen evolution electrocatalysts in acidic and alkaline medium, Carbon 171 (2021) 385–394, https://doi.org/10.1016/j.carbon.2020.09.037.

[41] Q. Du, R. Zhao, T. Guo, L. Liu, X. Chen, J. Zhang, J. Du, J. Li, L. Mai, T. Asefa, Highly dispersed Mo_2C nanodots in carbon nanocages derived from Mo-based xerogel: efficient electrocatalysts for hydrogen evolution, Small Methods 5 (2021), 2100334, https://doi.org/10.1002/smtd.202100334.

[42] C. Yang, K. Shen, R. Zhao, H. Xiang, J. Wu, W. Zhong, Q. Zhang, X. Li, N. Yang, Balance effect: a universal strategy for transition metal carbides to enhance hydrogen evolution, Adv. Funct. Mater. 32 (2022) 2108167, https://doi.org/10.1002/adfm.202108167.

[43] X. Fan, Y. Liu, Z. Peng, Z. Zhang, H. Zhou, X. Zhang, B.I. Yakobson, W.A. I. Goddard, X. Guo, R.H. Hauge, J.M. Tour, Atomic H-induced Mo_2C hybrid as an active and stable bifunctional electrocatalyst, ACS Nano 11 (2017) 384–394, https://doi.org/10.1021/acsnano.6b06089.

[44] H. Wei, Q. Xi, X. Chen, D. Guo, F. Ding, Z. Yang, S. Wang, J. Li, S. Huang, Molybdenum carbide nanoparticles coated into the graphene wrapping N-doped porous carbon microspheres for highly efficient electrocatalytic hydrogen

evolution both in acidic and alkaline media, Adv. Sci. 5 (2018), 1700733, https://doi.org/10.1002/advs.201700733.

[45] E. Bertran-Serra, S. Rodriguez-Miguel, Z. Li, Y. Ma, G. Farid, S. Chaitoglou, R. Amade, R. Ospina, J.-L. Andújar, Advancements in plasma-enhanced chemical vapor deposition for producing vertical graphene nanowalls, Nanomaterials 13 (2023) 2533, https://doi.org/10.3390/nano13182533.

[46] G. Farid, R. Amade, S. Chaitoglou, I. Alshaikh, R. Ospina, Y. Ma, E. Bertran-Serra, Efficient flexible electrodes for lithium-ion batteries utilizing well-dispersed hybrid Mo_2C nanoparticles on vertically-oriented graphene nanowalls, J. Alloy. Compd. 968 (2023), 172109, https://doi.org/10.1016/j.jallcom.2023.172109.